Scalable Varied-Density Clustering via Graph Propagation

Ninh Pham
University of Auckland
Auckland, New Zealand
ninh.pham@auckland.ac.nz

Yingtao Zheng
University of Auckland
Auckland, New Zealand
yzhe906@aucklanduni.ac.nz

Hugo Phibbs
University of Auckland
Auckland, New Zealand
hphi344@aucklanduni.ac.nz

Abstract

We propose a novel perspective on varied-density clustering for high-dimensional data by framing it as a label propagation process in neighborhood graphs that adapt to local density variations. Our method formally connects density-based clustering with graph connectivity, enabling the use of efficient graph propagation techniques developed in network science. To ensure scalability, we introduce a density-aware neighborhood propagation algorithm and leverage advanced random projection methods to construct approximate neighborhood graphs. Our approach significantly reduces computational cost while preserving clustering quality. Empirically, it scales to datasets with millions of points in minutes and achieves competitive accuracy compared to existing baselines.

1 Introduction

Density-based clustering [7] identifies clusters as dense regions separated by sparse areas, allowing it to detect arbitrarily shaped clusters and handle noise effectively. Unlike methods like k-means [27], it does not assume spherical clusters or require the number of clusters in advance, making it ideal for complex, real-world data.

Representative density-based clustering methods, such as DBSCAN [18] and Density Peak Clustering (DPC) [35], can be interpreted as *label propagation* mechanisms over a graph defined by local density relationships. In this view, clusters are seeded at high-density points–called core points in DBSCAN or density peaks in DPC–which act as the initial label sources. The labels are then propagated from high-to-low density regions, following the structure of a neighborhood graph, which typically assigns remaining points to the label of its near neighbor with similar densities. This formulation naturally respects the underlying density landscape: labels do not cross low-density regions, allowing the algorithm to discover non-convex clusters and separate noisy or sparse areas. Thus, clustering emerges from how labels flow along high-density paths in the neighborhood graph.

Considering each data point as a node in a graph, DBSCAN or DPC has two primary steps, including (1) constructing an ϵ-neighborhood or k-nearest neighbor (kNN) graph to discover density and neighborhood of each node, and (2) propagating cluster labels from dense nodes to sparse nodes. The first step is the main computational bottleneck as forming these neighborhood graphs requires a worst-case $O(n^2)$ time for a dataset of n points in high dimensions [29, 43]. This limits the applications of density-based clustering on modern million-point datasets. Prior work has tackled this issue by leveraging randomized techniques, such as random projections [36, 44], hashing [17, 31] or sampling [23, 25, 41], to approximate the graph construction. Other work [2, 12, 19, 22, 28] follow the prune-and-bound strategies based on geometric properties on metric spaces to reduce the number of ϵ-neighborhood queries while forming clusters.

While density-based clustering and its approximate variants are effective for discovering arbitrarily shaped clusters, they struggle on datasets with highly varied densities due to their reliance on global parameters. DBSCAN requires a fixed neighborhood radius (ϵ) and minimum points ($minPts$), which makes it difficult to capture clusters of different densities simultaneously: a setting that works for dense regions may cause sparse clusters to be missed or merged with noise. Similarly, DPC relies on a cutoff distance (d_c) to compute local density and to derive a decision graph to identify cluster centers, but distinguishing true peaks becomes ambiguous when density differences across clusters are extreme. As a result, both algorithms often fail to capture meaningful structures in heterogeneous data, due to their inability to adapt clustering behavior to various local density scales.

Several methods address this issue in datasets with varied densities by incorporating local density estimates derived from kNN distances [15, 16, 46] or dynamically adjusting the parameter ϵ based on the local neighborhood structure [4, 8] to overcome the limitations of global parameters in DBSCAN and DPC. While effective in capturing heterogeneous clusters, these methods often lack scalability, as they rely on constructing the exact kNN graph or performing exhaustive ϵ-neighborhood queries. These operations become computationally intensive on large, high-dimensional datasets, limiting their practicality in real-world applications.

Contribution. This work presents a best-of-both-worlds approach to density-based clustering that is both scalable and effective for large-scale, high-dimensional datasets with heterogeneous densities. We unify classical density-based clustering with a graph-based paradigm, replacing rigid density-connectivity rules with flexible label propagation conditions. Building on this connection, we introduce *PING* (Propagation In Neighborhood Graphs), a simple yet strong clustering baseline that combines recent advances in approximate nearest neighbor search (ANNS) with efficient label propagation techniques from network science. To overcome the computational bottlenecks of graph construction and propagation on large datasets, we propose a fast density-aware label propagation algorithm that avoids explicit graph materialization, along with a scalable strategy for constructing high-quality approximate neighborhoods. Together, these components make PING a scalable and effective solution for varied-density clustering in real-world, large-scale high-dimensional datasets.

Our Density-aware Neighborhood Propagation (*DNP*) algorithm identifies cluster centers as the highest density peaks and propagates their labels in descending density order through a neighborhood graph. The propagation prioritizes points that are both close to the cluster centers and locally dense, ensuring coherent expansion of clusters. By removing the reliance on a fixed-radius parameter, DNP provides greater flexibility and robustness in detecting clusters of varying shapes and density scales in heterogeneous

or high-dimensional datasets. DNP is particularly well-suited for approximate kNN graphs with large k due to its simplicity, deterministic nature, and computational efficiency.

We extend CEOs [32], a recent random projection method for approximate nearest neighbor search (ANNS), to efficiently approximate neighborhoods under cosine distance. Furthermore, we generalize CEOs to support other widely used distance measures—including L2, L1, χ^2, and Jensen–Shannon distances by leveraging random kernel feature mappings [34, 40]. Under mild assumptions on the data distribution, we theoretically demonstrate that CEOs preserves the graph connectivity necessary for recovering DBSCAN-like cluster structures across varying ε values.

Efficiency. Our proposed baseline, PING, combined with well-established label propagation algorithms such as Leiden [39] and Louvain [5], is simple yet effective–running significantly faster and achieving higher clustering accuracy than several existing methods on standard benchmarks. For instance, MNIST ($n = 70,000, d = 784$), PING achieves a **90% AMI** score in under **30 seconds**, outperforming DCN [45], a deep learning-based k-means approach, which reaches only **75% AMI** and requires more than **30 minutes** of computation.

Scalability. On MNIST8M (8.1 million points), our DNP completes clustering on outputs of ANNS solvers under **15 minutes** on a single machine with a 32-core 2.2GHz AMD CPU and 128GB RAM, achieving up to **72% NMI** score. In contrast, kernel k-means [42] gives only **41% NMI** on a Spark-based supercomputing cluster with 32 nodes–each node equipped with dual 16-core (32-thread) 2.3GHz Haswell CPUs and 128GB memory.

2 Related Work

Since our approach views density-based clustering as a label propagation process over a graph induced by local neighborhood relationships, we reinterpret classical density-based clustering algorithms within this unified framework.

Density-based clustering (DBSCAN) [18] identifies clusters as connected regions of high densities. Given a distance measure $d(\cdot,\cdot)$, DBSCAN is parameterized by a radius ε and a density threshold $minPts$. For each point $\mathbf{x}_i \in \mathbf{X}$, DBSCAN performs an *$\varepsilon$-range query* $B_\varepsilon(\mathbf{x}_i) = \{\mathbf{x}_j \in \mathbf{X} \mid d(\mathbf{x}_i, \mathbf{x}_j) \le \varepsilon\}$, and classifies $\mathbf{x}_i$ as a *core* point if $|B_\varepsilon(\mathbf{x}_i)| \ge minPts$; otherwise, it is considered a *non-core* point.

Clusters are formed by recursively connecting core points within mutual ε-neighborhoods. Non-core points within the neighborhood of a core point are labeled as border points and assigned the core point's cluster label. This process can be interpreted as propagating cluster labels across a graph where edges link core points within ε-distance. While effective for uniform-density clusters, DBSCAN's reliance on global parameters ε and $minPts$ limits its performance on datasets with varying densities.

Density Peak Clustering (DPC) [35] addresses DBSCAN's sensitivity to global parameters by incorporating a more adaptive density estimation. Given a cutoff distance d_c, DPC computes a local density score $\rho_i = |B_{d_c}(\mathbf{x}_i)|$, the number of points within distance d_c of $\mathbf{x}_i$. DPC identifies cluster centers as points with high local density ρ_i and large distance δ_i to any point of higher density, where $\delta_i = \min_{j:\rho_j > \rho_i} d(\mathbf{x}_i, \mathbf{x}_j)$. This metric captures both local density and isolation, allowing DPC to discover well-separated peaks without requiring a fixed density threshold.

Once cluster centers are selected, labels are propagated by assigning each remaining point to the same cluster as its nearest neighbor of higher density, effectively following the ascending density gradient. While DPC mitigates the rigidity of DBSCAN's fixed-radius criterion, its performance still hinges on the choice of d_c; a poorly chosen cutoff can distort density estimates, leading to incorrect cluster centers and ultimately suboptimal clustering results.

Ordering Points for Clustering Structure (OPTICS) [4] extends DBSCAN by producing an ordering of data points based on their *reachability distances*, enabling hierarchical cluster extraction across multiple density levels. Like DBSCAN, it relies on the notion of core points, but instead of forming flat clusters, OPTICS incrementally explores the data by prioritizing points that are density-reachable from known core points. Each point is assigned a reachability distance—the smallest distance needed to reach it from a core point—capturing how clusters unfold at different density scales. The resulting reachability plot reveals valleys corresponding to dense clusters, allowing users to extract meaningful clusterings without specifying a fixed global ε. However, OPTICS requires $O(n)$ ϵ-neighborhood search that are infeasible in large-scale high-dimensional datasets.

Label Propagation Algorithm (LPA) [33] is a widely used method for graph clustering and community detection, valued for its simplicity, efficiency, and ability to uncover densely connected structures without requiring the number of clusters in advance. Starting from a set of initial labels (often randomly assigned), the algorithm iteratively updates each node's label to the most frequent label among its neighbors. This local update rule typically converges rapidly to a stable partition in a few iterations. That makes LPA well-suited for large-scale data due to its low computational overhead (e.g. $O(kn)$ in a kNN graph with n nodes).

Louvain and Leiden are widely used community detection algorithms that build upon label propagation principles to identify *modular* structures in large-scale graphs. *Louvain* [5] greedily optimizes modularity [30] by moving each node to the neighboring community that yields the highest modularity gain, followed by aggregation of communities into super-nodes and repeating the process hierarchically. However, Louvain can get stuck in disconnected or poorly connected communities. *Leiden* [39] addresses this by introducing a refinement phase that guarantees intra-community connectivity. It iteratively improves the community structure by locally moving nodes based on a fast local update rule and then refining the partition using a more principled stability criterion before aggregation. Both algorithms naturally support weighted graphs by incorporating edge weights into the modularity computation, allowing them to capture fine-grained community structures where edge weights encode pairwise similarities of points, particularly beneficial in kNN graphs derived from real-world data.

Recent work has explored integrating Density Peak Clustering (DPC) with label propagation techniques [1, 38]. These hybrid approaches typically identify cluster centers based on local density estimates derived from variants of the kNN graph and then propagate labels from high-density nodes to their neighbors. While this formulation improves cluster assignment consistency and robustness across density gradients, it critically depends on constructing a

high-quality kNN graph that becomes computationally prohibitive for large-scale, high-dimensional datasets.

3 A Baseline via Asymptotic Equivalence of DBSCAN and Graph Connectivity

This section establishes theoretical conditions under which DBSCAN cluster structures, defined via ϵ-neighborhood graphs with varying ϵ values, can be recovered through the connectivity of *mutual* kNN graphs. These conditions enable the use of kNN-based graph constructions to approximate the behavior of DBSCAN under non-uniform densities by adapting neighborhood size implicitly through local point distributions. This connection lays the groundwork for recent approaches that recover density-based clustering using kNN graph variants [1, 15, 38, 46], providing both practical scalability and theoretical justification.

Given a dataset $\mathbf{X}$ of n points $\mathbf{x}_i \in \mathbb{R}^d$, the mutual kNN graph constructed on $\mathbf{X}$ is symmetric and has an edge $(\mathbf{x}_i, \mathbf{x}_j)$ if $\mathbf{x}_i \in \text{kNN}(\mathbf{x}_j)$ *and* $\mathbf{x}_j \in \text{kNN}(\mathbf{x}_i)$. We will use the following result to prove our main theorem regarding the equivalence of DBSCAN and kNN graph connectivity.

Theorem 1 (Connectivity of Mutual kNN Graph [6]). *Let $\mathbf{X} = \{\mathbf{x}_1, \ldots, \mathbf{x}_n\} \subset \mathbb{R}^d$ be i.i.d. samples drawn from a probability density function $f : \mathbb{R}^d \to \mathbb{R}_+$ with compact support. Let $\mathcal{L}_{f_0} = \{\mathbf{x} \in \mathbf{X} : f(\mathbf{x}) \geq f_0\}$ be a connected superlevel set of the density. Construct the* mutual *k-nearest neighbor graph G_k on $\mathbf{X}$, and let $G_k[\mathcal{L}_{f_0}]$ be the subgraph induced by points in $\mathcal{L}_{f_0}$.*

Then, if

$$k \geq c \log n$$

for some constant $c > 0$, it holds that with high probability as $n \to \infty$, the graph $G_k[\mathcal{L}_{f_0}]$ is connected.

We assume that the following hold:

(1) (Smoothness) f is Lipschitz continuous with constant $\alpha > 0$.
(2) (Cluster Structure) Clusters are defined as connected components of the superlevel set $\{\mathbf{x} : f(\mathbf{x}) \geq f_0\}$ for some threshold $f_0 > 0$.
(3) (Cluster Separation) Any path from one cluster to another must pass through a region where $f(\mathbf{x}) < f_0$.
(4) (Sampling) Let $d_k(\mathbf{x})$ be the kNN distance of $\mathbf{x}$ given $k = o(n)$ and $k \to \infty$ when $n \to \infty$.

The smoothness assumption ensures that nearby points in the same cluster will have similar density. The second and third ones ensure that the true clusters are located in high-density areas, and are separated away from noise regions with sufficiently low density. The last assumption ensures that the kNN-based density estimator $\widehat{f}(\mathbf{x})$ converges to the true density $f(\mathbf{x})$ almost surely. These assumptions are widely used to analyze density-based clustering algorithms [9, 24, 25, 44].

We define a *varied-density DBSCAN*, called $DBSCAN_k^*$, where we set $minPts = k$ and *sequentially* run DBSCAN using a series of increasing density thresholds $\epsilon_L < \epsilon_{L-1} < \ldots < \epsilon_1$, recovering density-based clusters $C_L, \ldots, C_1$ in order from the densest to the sparsest. At each stage, the algorithm operates on the set of non-core points from the previous run, allowing cluster discovery at progressively lower density levels. The following result establishes that the cluster structure induced by $DBSCAN_k^*$ can be recovered via connectivity in a mutual kNN graph. The proof that uses four assumptions mentioned above is left in the appendix.

Algorithm 1: PING: Propagation in Neighborhood Graphs

Input: $\mathbf{X} \subset \mathbb{R}^d$, k
1 For each point, find approximate kNN by any ANNS library
2 Build a weighted symmetric kNN graph G_k
3 **Return** Communities of G_k by Leiden or Louvain

Theorem 2 (DBSCAN Cluster Recovery via Mutual kNN Connectivity). *Let $\mathbf{X} = \{\mathbf{x}_1, \ldots, \mathbf{x}_n\} \subset \mathbb{R}^d$ be i.i.d. samples drawn from a Lipschitz continuous density function f, and let $\mathcal{L}_{f_0} = \{\mathbf{x} \in \mathbb{R}^d : f(\mathbf{x}) \geq f_0\}$ be a union of L disjoint, compact, connected components $\mathcal{L}_{f_i} = \{\mathbf{x} \in \mathbb{R}^d : f(\mathbf{x}) \geq f_i\}$, where $f_0 \leq f_1 < \ldots < f_L$, separated by low-density regions where $f(\mathbf{x}) < f_0$.*

Construct the mutual k-nearest neighbor graph G_k on $\mathbf{X}$, where $k \geq c \log n$ for a sufficiently large constant $c > 0$. Run $DBSCAN_k^*$ with L density thresholds $\epsilon_i = (k/nV_d f_i)^{1/d}$ where V_d denotes the volume of the unit ball in $\mathbb{R}^d$.

Then, with high probability as $n \to \infty$:

- *The mutual kNN graph G_k is connected within each high-density component $\mathcal{L}_{f_i}$ corresponding to the cluster C_i.*
- *The clusters of $DBSCAN_k^*$ can be recovered asymptotically by identifying connected components of core points in G_k.*

Theoretically, Theorem 2 implies that a simple label propagation procedure–starting from a randomly selected high-density point and propagating its label to all reachable points in the mutual kNN graph–can recover the clustering structure produced by $DBSCAN_k^*$ with high probability. This observation leads to a practical and conceptually simple clustering baseline based solely on graph connectivity and local density, without requiring the number of clusters to be specified–unlike k-means-based methods [27, 37, 42, 45].

PING: A clustering baseline via propagation in neighborhood graphs. We study the *weighted symmetric* kNN graph where the edge $(\mathbf{x}_i, \mathbf{x}_j)$ exists if either $\mathbf{x}_i \in \text{kNN}(\mathbf{x}_j)$ or $\mathbf{x}_j \in \text{kNN}(\mathbf{x}_i)$ and is assigned a weight equal to $d(\mathbf{x}_i, \mathbf{x}_j)$. As a natural superset of the mutual kNN graph, the symmetric kNN graph retains the key connectivity properties needed to capture core point structures within density-based clusters. Moreover, its denser connectivity structure improves robustness on datasets with varied densities, where mutual kNN graphs may fragment. Importantly, symmetric kNN graphs can be constructed efficiently at scale by leveraging state-of-the-art ANNS libraries such as Faiss [14].

Another benefit of using the weighted symmetric kNN graph is the ability to leverage *weight-aware modularity* in advanced label propagation algorithms such as Leiden [39] and Louvain [5]. These algorithms optimize modularity by favoring tighter communities when nodes are connected by smaller distances–naturally aligning with clustering objectives. Algorithm 1 outlines our simple PING baseline built on this idea.

While the theoretical assumptions, such as smooth density within clusters and large inter-cluster gaps, may not hold in real-world datasets, Leiden and Louvain remain remarkably efficient and effective. For example, on Mnist $n = 70,000, d = 784$, both algorithms

Algorithm 2: DNP: Density-aware neighborhood propagation

Input: Data points $\mathbf{X}$, the set $kNN(\mathbf{q})$ and its corresponding kNN distance for each point $\mathbf{q} \in \mathbf{X}$
Output: Cluster labels $L = \{l_1, \ldots, l_n\}$

Initialize labels: $L[\mathbf{q}] \leftarrow -1$ for all $\mathbf{q}$
Initialize reachability-distance : $reachDist[\mathbf{q}] \leftarrow \infty$ for all $\mathbf{q}$
Sort $\mathbf{q}$ based on its estimated density $1/d_k(\mathbf{q})$
Initialize priority queue Q, $nClust = -1$
foreach $\mathbf{q} \in \mathbf{X}$ *in the sorted density order* **do**
  if $L[\mathbf{q}] > -1$ **then**
    continue
  $nClust = nClust + 1$; $L[\mathbf{q}] \leftarrow nClust$
  foreach $\mathbf{q}' \in kNN(\mathbf{q})$ **do**
    if $L[\mathbf{q}'] = -1 \wedge d(\mathbf{q}, \mathbf{q}') < reachDist[\mathbf{q}']$ **then**
      `% Update reachability-distance`
      $reachDist[\mathbf{q}'] \leftarrow d(\mathbf{q}, \mathbf{q}')$
      Insert $\mathbf{q}'$ and its predecessor $\mathbf{q}$ with the priority $d(\mathbf{q}, \mathbf{q}') + d_k(\mathbf{q}')$ into Q
  while Q *is not empty* **do**
    Pop $(\mathbf{x}, \mathbf{p}, \_)$ from Q `% p is predecessor of x`
    if $L[\mathbf{x}] = -1$ **then**
      if $\exists\, \mathbf{x}' \in kNN(\mathbf{x})$ *such that* $L[\mathbf{x}'] = L[\mathbf{p}]$ **then**
        $L[\mathbf{x}] \leftarrow L[\mathbf{p}]$ `% Use predecessor label`
      else
        `% x forms a new cluster`
        $nClust = nClust + 1$; $L[\mathbf{x}] \leftarrow nClust$
      foreach $\mathbf{x}' \in kNN(\mathbf{x})$ **do**
        if $L[\mathbf{x}'] = -1 \wedge d(\mathbf{x}, \mathbf{x}') < reachDist[\mathbf{x}']$ **then**
          `% Update reachability-distance`
          $reachDist[\mathbf{x}'] \leftarrow d(\mathbf{x}, \mathbf{x}')$
          Insert $\mathbf{x}'$ and its predecessor $\mathbf{x}$ with the priority $d(\mathbf{x}, \mathbf{x}') + d_k(\mathbf{x}')$ into Q
Return L

combined with Faiss-IVF achieve **90% AMI** in under **30 seconds**, outperforming DCN [45], a deep learning based approach that takes over **30 minutes** to reach **75% AMI**.

4 Scalable Varied-density Clustering

While *PING* demonstrates high efficiency and accuracy on small datasets, it faces two key computational bottlenecks when applied to large-scale data. First, Leiden and Louvain tend to converge slowly on datasets with millions of points, particularly when larger values of k are required for accurate clustering. Second, building the ANNS index and performing n approximate kNN queries become increasingly expensive in high-dimensional settings. In the following sections, we address each of these bottlenecks with targeted algorithmic improvements.

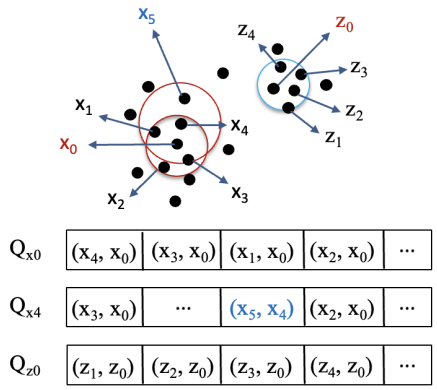

Figure 1: An illustration of DNP.

4.1 Density-aware neighborhood propagation

Motivated by the observation that symmetric kNN graphs are typically well-connected in high-density regions, we replace the expensive modularity-based optimization of Leiden and Louvain with a fast, greedy heuristic tailored to density-based clustering. We introduce a *deterministic* label propagation algorithm, called *Density-aware Neighborhood Propagation (DNP)*, which initiates clustering from the highest-density point and propagates labels to nearby, lower-density neighbors along descending density gradients. DNP can be interpreted as a principled method for extracting clusters from the OPTICS dendrogram, where cluster formation begins from the deepest valleys and proceeds through density-reachable paths. Empirically, DNP avoids the overhead of graph materialization and modularity optimization, running significantly faster than Leiden and Louvain while maintaining comparable clustering accuracy.

Algorithm 2 outlines the procedure of our *Density-aware Neighborhood Propagation (DNP)* algorithm. DNP initiates clustering from the highest-density point $\mathbf{q}$, where density is estimated using the inverse kNN distance, $1/d_k(\mathbf{q})$. It then propagates the label $L[\mathbf{q}]$ to unlabeled neighbors $\mathbf{q}'$, prioritizing candidates based on a *composite* score: $d(\mathbf{q}, \mathbf{q}') + d_k(\mathbf{q}')$. This priority function favors nearby points ($d(\mathbf{q}, \mathbf{q}')$) with high local density ($d_k(\mathbf{q}')$), ensuring that label propagation respects both spatial proximity and density gradients.

A point $\mathbf{q}'$ is eligible to receive a label if at least one of its k nearest neighbors has already been assigned the label $L[\mathbf{q}]$. To ensure propagation adheres to the true cluster structure, DNP maintains a best-so-far reachability distance:

$$\text{reachDist}(\mathbf{q}') = \min_{\mathbf{q} \text{ labeled},\ \mathbf{q}' \in \text{kNN}(\mathbf{q})} d(\mathbf{q}, \mathbf{q}'),$$

which guarantees that each point is labeled only by its closest labeled predecessor of higher density.

This two-fold prioritization–favoring both descending density and spatial proximity–combined with the use of the smallest reachability distance, ensures that label propagation follows the intrinsic structure of the data: *from high-to-low density regions* and *from near-to-far neighbors*. This disciplined propagation strategy mitigates the risk of label diffusion across low-density gaps, enabling clusters to grow coherently from dense cores.

Algorithm 3: CEOs: Find approximate neighborhoods

Input: $\mathbf{X} \subset \mathcal{S}^{d-1}$, two set of D random vectors $\mathbf{R}, \mathbf{S}$, $s, m = O(k)$

% Build index

1 **foreach** $\mathbf{q} \in \mathbf{X}$ **do**

2 Compute and store top-s closest vectors $\mathbf{r}_i \in \mathbf{R}$ and top-s closest vectors $\mathbf{s}_j \in \mathbf{S}$ to $\mathbf{q}$

3 Hash $\mathbf{q}$ into these top-s^2 buckets B_{ij} corresponding to $\mathbf{z}_{ij} = \mathbf{r}_i + \mathbf{s}_j$

4 **foreach** *bucket* B_{ij} *corresponding to* $\mathbf{z}_{ij}$ **do**

5 If $|B_{ij}| \geq m$, keep top-m points $\mathbf{x}_i$ with largest $\mathbf{x}_i^\top \mathbf{r}_i + \mathbf{x}_i^\top \mathbf{s}_j$ (i.e. closest to $\mathbf{z}_{ij}$)

% Find approximate neighborhood

6 **foreach** $\mathbf{q} \in \mathbf{X}$, initialize an empty neighborhood set $N(\mathbf{q})$

7 **foreach** $\mathbf{q} \in \mathbf{X}$ **do**

8 **foreach** *bucket* B_{ij} *corresponding to top-*s *vector* $\mathbf{z}_{ij}$ *closest to* $\mathbf{q}$ **do**

9 **foreach** $\mathbf{x} \in B_{ij}$ **do**

10 Insert $(\mathbf{x}, \mathbf{x}^\top \mathbf{q})$ into $N(\mathbf{q})$

11 Insert $(\mathbf{q}, \mathbf{x}^\top \mathbf{q})$ into $N(\mathbf{x})$

12 **foreach** $\mathbf{q} \in \mathbf{X}$, sort its neighbors $N(\mathbf{q})$ by the dot product

13 **Return** $N(\mathbf{q})$ for each $\mathbf{q} \in \mathbf{X}$

An illustrative example of DNP process with $k = 4$ is shown in Figure 1. The highest density point $\mathbf{x}_0$ creates a new cluster. Its 4 nearest neighbors $\mathbf{x}_4, \mathbf{x}_3, \mathbf{x}_1, \mathbf{x}_2$ are added to Q with the corresponding priority score together with their predecessor $\mathbf{x}_0$. When processing $\mathbf{x}_4$, $\mathbf{x}_3$ (and $\mathbf{x}_1$) will not be added as $d(\mathbf{x}_4, \mathbf{x}_3) > d(\mathbf{x}_0, \mathbf{x}_3)$. $\mathbf{x}_5$ is added to Q with a higher priority than $\mathbf{x}_2$. Though we might grow the cluster towards the direction of $\mathbf{x}_5$, by keeping the predecessor $\mathbf{x}_0$, $\mathbf{x}_2$ can still be labeled correctly. Though $\mathbf{z}_0$ might be reached by any $\mathbf{x}_i$, it will not be labeled as its kNN have not been labeled yet. When Q is empty, the next highest density point, e.g., $\mathbf{z}_0$, is processed, creating a new cluster. Its neighbors will be added to Q. The process will continue until all points are labeled.

Time complexity and practical considerations. Given the input graph G_k, the proposed DNP algorithm is deterministic and runs in $O(nk \cdot \log(nk))$ time as the size of priority queue Q is bounded by nk. As DNP is significantly faster than modularity-based methods in practice, it can be operated effectively even on graphs with large k. However, for large k, the kNN distance $d_k(\mathbf{q})$ becomes less indicative of the true local density at point $\mathbf{q}$. To mitigate this, we propose a (c, k)-parameterized DNP that uses $d_{k'}(\mathbf{q})$, where $k' = k/c$ for a small constant $c \geq 1$, as the local density and the density component in the propagation priority. The (c, k)-parameterized DNP is especially important when combined with ANNS, as the approximation error in d_k tends to grow with large k, potentially distorting density estimation. Indeed, the constant c modulates the trade-off between capturing local density variations and ensuring robust neighborhood connectivity.

4.2 Approximate neighborhoods via CEOs

Clustering via graph propagation relies critically on the connectivity of the underlying neighborhood graph. To this end, we extend CEOs [32], a recent random projection-based method that leverages the concomitants of extreme order statistics to approximate the nearest neighbors of each point. Our theoretical analysis shows that, under mild regularity assumptions on the data distribution, the neighborhood graph constructed by CEOs remains connected within high-density regions with high probability on *cosine* distance. Consequently, this graph structure enables recovery of DBSCAN-like cluster structures with varying ϵ values. The extension to L1, L2, Jensen-Shannon and χ^2 distance measures via random kernel feature mappings [34, 40] is left in the appendix.

We consider two independent sets of random projection vectors $\mathbf{R} = \{\mathbf{r}_1, \ldots, \mathbf{r}_D\}, \mathbf{S} = \{\mathbf{s}_1, \ldots, \mathbf{s}_D\}$, where the coordinates of each vector $\mathbf{r}_i, \mathbf{s}_j$ are randomly selected from $N(0, 1)$. For each pair of random vectors $(\mathbf{r}_i, \mathbf{s}_j)$, we define a composite projection direction $\mathbf{z}_{ij} = \mathbf{r}_i + \mathbf{s}_j$, and associate it with a bucket B_{ij} storing the top-m points $\mathbf{x} \in \mathbf{X}$ with the largest score $\mathbf{x}^\top \mathbf{z}_{ij} = \mathbf{x}^\top \mathbf{r}_i + \mathbf{x}^\top \mathbf{s}_j$. This process can be executed efficiently by computing the top-s closest vectors in $\mathbf{R}$ and the top-s closest vectors in $\mathbf{S}$ to $\mathbf{q}$, hashing $\mathbf{q}$ into these s^2 buckets (Lines 2–3), and trimming the bucket if its size is larger than m (Line 5).

To approximate neighborhoods of $\mathbf{q}$, we select its top-s composite directions $\mathbf{z}_{ij}$ and retrieving their corresponding buckets. Since each bucket is truncated to the top-m candidates to limit memory and runtime, the final candidate set, of size $O(sm)$, is re-ranked to approximate the k-nearest neighbors of $\mathbf{q}$.

This method extends sDBSCAN [44] by introducing a two-level projection mechanism inspired by concomitant of extreme order statistics (CEOs), enhancing approximation accuracy with minimal computational overhead. The hash-based structure enables scalable and density-sensitive neighborhood construction while preserving the high-density connectivity required for clustering.

Our approximate neighborhood construction procedure is summarized in Algorithm 3. Since each query yields an approximate neighborhood of size $O(sm)$, we denote the resulting graph as G_{sm}. From G_{sm}, we can construct an approximate weighted symmetric kNN graph G_k for any $k = o(sm)$.

Time and space complexity. We will use the Structured Spinners [3] that exploits Fast Hadamard Transform (FHT) to simulate the cost of Gaussian random projections with $O(D \log D)$ time with $O(D)$ additional space. Given a constant s and $m = O(k) \ll n$, the time complexity of Algorithm 3 is $O(nD \log D + dn \cdot m)$. The space complexity is $O(m \cdot D^2 + n \cdot m)$, where the first term corresponds to the index with D^2 buckets, and the last term is the memory of the output graph G_{sm}. In practice, the distance computation and the memory footprint to store $N(\mathbf{q})$ for each $\mathbf{q} \in \mathbf{X}$ dominate the complexity, so setting $D \approx \sqrt{n}, m = O(k)$ will balance the cost.

Practical considerations. Both indexing and querying phases of CEOs are elementary to run in parallel, and our multi-threading implementation shows a 12× speedup with 32 threads. When processing the point $\mathbf{q}$, the combination method CEOs-DNP adds all points $\mathbf{q}' \in N(\mathbf{q})$, instead of $kNN(\mathbf{q})$, to the priority queue Q to leverage all computed neighbors. The rest of the the process of (c, k)-parameterized DNP is still the same.

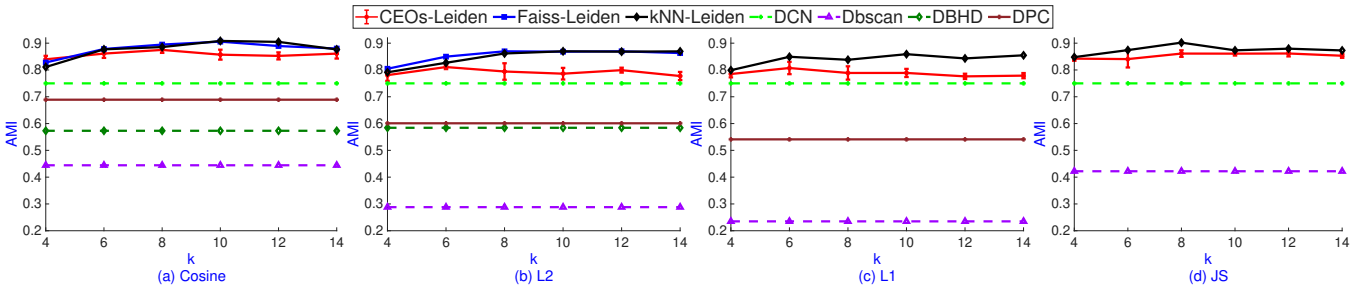

Figure 2: The AMI comparison of PING (CEOs, FaissIVF, and exact kNN for graph constructions with Leiden) and other clustering competitors. We report the *best* AMI scores of compared competitors after tuning their parameters.

Table 1: The total runtime and finding kNN time in 32 threads, and the accuracy of CEOs, Faiss-IVF, and exact kNN in seconds with Leiden on cosine. CEOs uses $D = 128, s = 20, m = 50, k = 8$. Leiden takes 11 seconds.

Alg.	Runtime (s)	kNN time (s)	AMI	CC
CEOs	**14**	**3 (21% of total)**	88% ± 1%	86% ± 1%
Faiss	34	23 (68% of total)	89%	87%
Exact	101	90 (89% of total)	90%	88%

4.3 Theoretical analysis

This subsection presents our theoretical analysis to ensure the connectivity of the graph constructed by CEOs.

W.l.o.g., we assume $\mathbf{x}_k$ and $\mathbf{x}_m$ are top-k and top-m nearest neighbors of $\mathbf{q}$ in $\mathbf{X}$, respectively, for $m > k$.

Let $\alpha_* = \arg\min_{\mathbf{q}\in\mathbf{X}} \left(\mathbf{q}^\top\mathbf{x}_k - \mathbf{q}^\top\mathbf{x}_m\right) / \left(\sqrt{1-(\mathbf{q}^\top\mathbf{x}_k)^2} + \sqrt{1-(\mathbf{q}^\top\mathbf{x}_m)^2}\right)$.

Given some assumption in independence, the following lemma justifies that kNN($\mathbf{q}$) are among $O(sm)$ candidate points returned by CEOs with high probability. The proof is similar to [44, Appendix B] and left in the appendix.

Lemma 3. *Given $D = n^{1/s\cdot\alpha_*^2}$ for a given point $\mathbf{q} \in \mathbf{X} \subset \mathcal{S}^{d-1}$, $kNN(\mathbf{q})$ are among $O(sm)$ points associated to the top-s closest random vectors $\mathbf{z}_{ij}$ to $\mathbf{q}$ with probability at least $p = e^{-k/n}$.*

We use the following lemma to guarantee the connectivity of subgraphs corresponding to high-density areas provided by CEOs.

Lemma 4. *[26] Let G be a graph of n vertices with min-cut t and $0 < \delta < 1$. There exists a universal constant c such that if $s \geq \frac{c(\log(1/\delta)+\log(n))}{t}$, then with probability at least $1-\delta$, the graph G' derived by sampling each edge of G with probability s is connected.*

Let $DBSCAN_k^*$ produce L disconnected components $\mathcal{L}_{f_1}, \ldots, \mathcal{L}_{f_L}$ corresponding to corresponding to L clusters $C_1, \ldots, C_L$. Similar to [25, 44], we assume that there exists a constant $t > 0$ such that, for any edge $(\mathbf{x}_1, \mathbf{x}_2) \in G_k$, we have $|B_{d_k(\mathbf{x}_1)}(\mathbf{x}_1) \bigcap B_{d_k(\mathbf{x}_2}(\mathbf{x}_2)| \geq t$, and assume that t will not be small on high-density areas. By applying Lemma 4 on each $\mathcal{L}_{f_i}$, we state our main result.

Theorem 5. *Let $\mathcal{L}_{f_1}, \ldots, \mathcal{L}_{f_L}$ be connected subgraphs produced by $DBSCAN_k^*$ where each $\mathcal{L}_{f_i}$ corresponds to a cluster C_i with n_i core points. Assume that any edge $(\mathbf{x}_1, \mathbf{x}_2) \in \mathcal{L}_{f_i}$ such that $B_{d_k(\mathbf{x}_1)}(\mathbf{x}_1)$ and $B_{d_k(\mathbf{x}_2)}(\mathbf{x}_2)$ share at least t common nodes. There exists a constant c such that if $te^{-k/n} \geq c(\log(1/\delta) + \log(n_i))$ for $i \in [l]$, each component $\mathcal{L}_{f_i}$ are still connected with probability at least $1-\delta$.*

Theorem 5 indicates that when the cluster C_i of n_i nodes is strongly connected, i.e. the common neighborhood of any two connected nodes has size at least $t = O(\log(n_i))$, the corresponding graph $\mathcal{L}_{f_i}$ is still connected in G_{sm} with probability $1 - 1/n_i$.

5 Experiment

We implement CEOs and DNP in C++ [1] and compile with `g++ -O3 -std=c++17 -fopenmp -march=native`. We conducted experiments on Ubuntu 20.04.4 with an AMD Ryzen Threadripper 3970X 2.2GHz 32-core processor with 128GB of DRAM. We use **`Faiss`** [14] and **`igraph`** [10], highly-optimized industry libraries, implemented in C/C++ in our PING baselines. We use 32-thread Faiss-IVF and Faiss-IVFPQ for ANNS and `igraph` for graph propagation algorithms, including Leiden, Louvain, and the standard LPA. Faiss-IVF offers higher accuracy than Faiss-IVFPQ but indexing and querying are much slower. Both igraph and our DNP do not support multi-threading.

We present empirical evaluations on the clustering quality compared to the ground truth (i.e. data labels) to verify our claims:

- Our baseline PING is very competitive in term of runtime and accuracy compared to existing strong baselines with their *tuned* parameters.
- CEOs runs faster than Faiss, a widely-used ANNS library, outputting the graph G_{sm} that returns comparable clustering accuracy with Leiden and Louvain.
- DNP runs significantly faster than Leiden and Louvain, and offers comparable accuracy on million-point datasets.
- CEOs+DNP offers superior running time while maintaining higher accuracy compared to other density-based clustering on million-point datasets.

We use popular metrics, including AMI, NMI, ARI, CC [20] to measure the clustering quality. We mainly report AMI scores in the paper. Results on other metrics are left in the appendix. We conduct experiments on three popular data sets: Mnist ($n = 70,000, d = 784$, # clusters = 10), Pamap2 ($n = 1,770,131, d = 51$, # clusters = 18), and Mnist8m ($n = 8,100,000, d = 784$, # clusters = 10). All results are the average of 5 runs of the algorithms.

[1] The code with Python wrapper will be released after the review process.

Table 2: The AMI and 32-thread runtime comparison of CEOs-Leiden with $k = 8$ and several clustering competitors on cosine distance. We report the *best* AMI scores of compared competitors after tuning their parameters.

Alg.	CEOs-Lei	sDbscan	Dbscan	Optics	HDBSCAN	DPC	DBHD	SpectACl	SC	KKM	k-means	DCN
AMI	**88% ± 1%**	42% ± 4%	43%	6%	31%	69%	56%	80%	50%	54%	51%	75%
# clusters	**12 ± 0.7**	29 ± 6	7	47	9	12	118	–	–	–	–	–
Time	14s	3s	34s	25 min	1 hour	5 min	> 2 hour	15s	1s	17s	1s	37 min

Table 3: Comparison on label propagation algorithms: DNP, LPA, Louvain, and Leiden over graph outputs by CEOs with $D = 256, s = 20, m = 50, k = 8$. CEOs runs in 2.7 s.

Alg.	Leiden	Louvain	LPA	DNP
Total time (s)	13.8	14.4	10.9	**3.7**
Clustering time (s)	11.1	11.7	8.2	**1**
AMI	88% ± 1%	85 % ± 2%	71% ± 1%	77% ± 2%
# clusters	12 ± 1	13 ± 1	227 ± 21	14 ± 2

Our competitors include (1) representative density-based clustering algorithms that do not need the predefined number of clusters, including DBSCAN [18], DPC [35], HDBSCAN [8], OPTICS [4], DBHD [16], sngDBSCAN [25], sDBSCAN [44]; and (2) representative clustering algorithms that need a predefined number of clusters, including k-means, kernel k-means (KKM), spectral clustering (SC), SpectACl [21], deep learning-based DCN [45]. Details of tuned parameter values of these algorithms are in the appendix.

5.1 An ablation study on Mnist

This subsection studies the performance of our proposed methods, including the baseline PING, the density-aware neighborhood propagation DNP, and the approximation neighborhood graph G_{sm} returned by CEOs. While our method does not need much parameter tuning, other competitors require a careful selection of parameter values to achieve reasonable accuracy. We detail the process of selecting parameter values of competitors in the appendix.

We run experiments to evaluate the performance of PING and the efficiency of CEOs compared to Faiss-IVF with $nlist = 100, nprobe = 10$ on Mnist. We report AMI score using Leiden. The results of Louvain are very similar and left in the appendix.

Comparison between PING baselines (CEOs, Faiss-IVF, and exact kNN with Leiden) and other clustering baselines. Figure 2 shows the AMI scores of the exact kNN, Faiss-IVF and CEOs with Leiden over a wide range of k. CEOs uses $D = 128, s = 20, m = 50$. For other selected clustering algorithms, including DBSCAN, DBHD, DPC, DCN, we report the *highest* AMI scores after several runs with different values of parameters. It is clear that our proposed PING baselines outperform other clustering competitors on several distance measures. In particular, they achieve at least 10%, 15%, 20%, and 45% higher AMI scores compared to DCN, DPC, DBHD, and DBSCAN, respectively.

Compared to exact kNN, our proposed CEOs suffers small loss in accuracy, with up to 5% on L2 and L1 due to the error caused by random kernel features. On cosine and JS, CEOs nearly reaches the accuracy of Faiss-IVF and exact kNN with less than 2% AMI loss.

Table 1 shows the detailed runtime comparison of different graph construction methods, including CEOs, Faiss-IVF, and exact kNN on cosine distance. CEOs uses $D = 256, s = 20, m = 50$. Though we use $D = 256$, the runtime of CEOs is nearly identical to the case of $D = 128$ since the main computation of CEOs is from distance computations, as detailed in the appendix.

The graph construction by CEOs runs significantly faster, up to 8× and 30×, compared to Faiss-IVF and exact kNN while preserving similar AMI and CC scores. Since Leiden takes 11 sec, CEOs is not the computational bottleneck as it constitutes to only 21% total time. However, the graph construction by Faiss-IVF is clearly the bottleneck with 68% total cost.

Comparison between CEOs-Leiden with other clustering baselines. Table 2 provides a systematic evaluation of CEOs-Leiden regarding runtime and accuracy on cosine distance compared to existing baselines, including density-based clustering without predefined number of clusters (sDBSCAN, DBSCAN, OPTICS, HDBSCAN DPC, DBHD) and other clustering with predefined number of clusters (SpecACl, SC, KKM, k-means, and DCN). Again, CEOs with Leiden offers superior performance in both time and accuracy compared to studied baselines. It runs in 14 seconds, slower than sDbscan and k-means but achieve nearly 40% higher AMI. Compared to the rest, CEOs-Leiden gives 8%, 13%, 20%, and more than 35% higher AMI than SpectACl, DCN, DPC, and the others, respectively. CEOs-Leiden also runs significantly faster than the others, offers 21×, and 130×, compared to DPC and DCN, respectively.

Comparison between DNP and Leiden, Louvain, LPA on CEOs's graphs. Table 3 shows detailed comparison regarding runtime and accuracy of 4 label propagation algorithms. Leiden, Louvain, and LPA run on top of the kNN graphs derived by G_{sm}, while (c, k)-DNP runs on G_{sm} with $c = 1$. It is clear that DNP runs significantly faster than modularity-based algorithms. Though it suffers around 10% loss in accuracy compared to Leiden and Louvain, its average AMI score 77% is still higher than non-graph propagation clustering competitors in Table 2 and run significantly faster than majority of them. DNP runs nearly 10× and 8× faster than modularity-based algorithms and LPA, respectively, while achieving higher accuracy than LPA. The speedup of DNP over Leiden and Louvain will be highlighted on million-point datasets Pamap2 and Mnist8m in the next subsections.

5.2 Experiments on Pamap2 and Mnist8m

This subsection run experiments to compared the performance of Faiss-IVF, Faiss-IFVPQ, and CEOs with propagation algorithms. CEOs uses $D = 512, m = 50$, and $s = \{20, 10\}$ on Pamaps and

Table 4: The AMI and runtime of PING instances and other clustering methods using L2 on Pamap2. Leiden and Louvain use $k = 12$ with Faiss variants. We report the *best* AMI scores of Dbscan variants after tuning their parameters.

Alg.	Faiss-IVF			Faiss-IVFPQ			CEOs-DNP	Dbscan	sDbscan	sngDbscan	k-means
	Leiden	Louvain	DNP	Leiden	Louvain	DNP					
AMI	**54%**	**54%**	52%	50%	50%	45%	48% ±0.5%	47%	44% ± 1.5%	38%	36%
Time (min)	5.3	5.7	2.1	3.7	3.3	1.4	**1**	30	**1**	3	3 sec

Table 5: The AMI and runtime of PING instances and other clustering methods with tuned parameters with cosine on Mnist8m.

Alg.	Leiden		Louvain		DNP		sDbscan-1NN	sDbscan	sngDbscan	Kernel
	$k = 10$	$k = 20$	$k = 10$	$k = 20$	Faiss	CEOs				k-means
AMI	54%	**73%**	55%	**73%**	72%	66%	38%	32%	26%	–
NMI	55%	**73%**	55%	**73%**	72%	66%	38%	32%	26%	41%
Time (min)	37	57	33	60	15	**7**	21	16	42	15

Mnist8m. sDbscan variants use $k = 10, minPts = 100$, which shares similar running time with CEOs and sngDbscan. Both use $\sigma = 40$, the average pairwise L2 distances, and $d' = 1024$ random features.

Pamap2. We present the representative results in L2, and leave results in L1 in the appendix. For Faiss variants, we use $nlist = 512, nprobe = 10$, and $m = 3$ for number of subquantizers. For Leiden and Louvain, we observe that $k = 12$ give the highest AMI scores. Larger k will increase its running time without increasing AMI due to the cost of modularity evaluations.

Conversely, DNP can run with a significantly larger values of k with a negligible runtime increase as Faiss and CEOs need a candidate size larger than k to answer ANNS with a high accuracy. This feature is especially useful in Faiss-IVFPQ and CEOs where these methods do not give high-quality kNN graphs compared to Faiss-IVF. Hence, (c, k)-DNP uses G_k where $k = \{25, 250\}$, and accordingly $k' = \{5, 50\}$ with $c = 5$ for Faiss-IVF and Faiss-IVFPQ. (c, k)-DNP runs on G_{sm} with $k = 75, c = 5$. The breakdown cost of different components, including finding kNN, forming the weighted graph, and propagation and parameter sensitivities on c and k of DNP are left in the appendix.

Table 4 shows a comparison in AMI and the runtime of several PING variants, including Faiss-IVF, Faiss-IVFPQ with Leiden, Louvain, DNP, CEOs-DNP, and DBSCAN variants. It shows that DNP suffers a small loss in accuracy but runs nearly 3× faster than Leiden and Louvain on Faiss variants. The combination of CEOs-DNP outperforms DBSCAN variants in term of accuracy and speed.

Mnist8m. Since we cannot run Faiss-IVF on our machine, we report the results of Faiss-IVFPQ, CEOs, and recent scalable density-based clustering, including sDbscan, sDbscan-1NN, sngDbscan, and the kernel k-means [42] run on a supercomputer with 32 nodes. As Leiden and Louvain run very slow on Mnist8m, we report representative results with $k = \{10, 20\}$ on cosine. Results on other values of k are in the appendix.

Table 5 shows the comparison between Faiss-IVFPQ and CEOs with different propagations, including Leiden, Louvain, and DNP on Mnist8m with cosine distance. Faiss-IVFPQ uses $nlist = 1024$, $nprobe = 10$, $m = 8$. CEOs uses $D = 512, s = 10, m = 50$. (c, k)-DNP uses $k' = 30$ and $c = \{5, 20\}$ for Faiss and CEOs. Again, DNP runs significantly faster than modularity-based methods and achieves comparable accuracy. DNP-based clustering outperforms non-propagation-based ones in both accuracy and speed. Table 5 shows the breakdown cost of different components of PING variants, highlighting the efficiency and scalability of DNP and CEOs.

Table 6: Breakdown runtime of Faiss-IVFPQ and CEOs with different propagation algorithms using cosine on Mnist8m.

Alg.	Faiss-Leiden		Faiss-DNP	CEOs-DNP
	$k = 10$	$k = 20$		
Find kNN (min)	12.7	12.7	13.1	3.8
Build graph (min)	12.1	23.9	0	0
Propagation (min)	9.2	20.4	2.2	2.8
Total time (min)	34	57	15.3	**6.6**
AMI	54%	73%	72%	66%

6 Conclusion

Our work bridges the gap between density-based clustering and graph-based learning by presenting a theoretically grounded and computationally efficient framework that scales to modern high-dimensional datasets. By unifying approximate kNN graph construction with label propagation, our approach provides a robust and scalable solution for clustering data with complex, heterogeneous structures. In particular, our novel density-aware neighborhood propagation method combined with advanced approximate nearest neighbor search (ANNS) solvers delivers strong empirical performance on million-point datasets.

Acknowledgments

Ninh Pham is supported by Marsden Fund (MFP-UOA2226). Yingtao Zheng is supported by China Scholarship Council (CSC).

References

[1] 2024. DPC-DNG: Graph-based label propagation of k-nearest higher-density neighbors for density peaks clustering. *Applied Soft Computing* 161 (2024), 111773.

[2] Daichi Amagata and Takahiro Hara. 2021. Fast density-peaks clustering: multicore-based parallelization approach. In *Proceedings of the 2021 International Conference on Management of Data*. 49–61.

[3] Alexandr Andoni, Piotr Indyk, Thijs Laarhoven, Ilya P. Razenshteyn, and Ludwig Schmidt. 2015. Practical and Optimal LSH for Angular Distance. In *NIPS*. 1225–1233.

[4] Mihael Ankerst, Markus M. Breunig, Hans-Peter Kriegel, and Jörg Sander. 1999. OPTICS: Ordering Points To Identify the Clustering Structure. In *SIGMOD*. 49–60.

[5] Vincent D Blondel, Jean-Loup Guillaume, Renaud Lambiotte, and Etienne Lefebvre. 2008. Fast unfolding of communities in large networks. *Journal of statistical mechanics: theory and experiment* 2008, 10 (2008), P10008.

[6] Mario R Brito, Edgar Chavez, Abel J Quiroz, and Joseph E Yukich. 1997. Connectivity of the mutual k-nearest-neighbor graph in clustering and outlier detection. *Statistics & Probability Letters* 35, 1 (1997), 33–42.

[7] Ricardo J. G. B. Campello, Peer Kröger, Jörg Sander, and Arthur Zimek. 2020. Density-based clustering. *WIREs Data Mining Knowl. Discov.* 10, 2 (2020).

[8] Ricardo J. G. B. Campello, Davoud Moulavi, Arthur Zimek, and Jörg Sander. 2015. Hierarchical Density Estimates for Data Clustering, Visualization, and Outlier Detection. *ACM Trans. Knowl. Discov. Data* 10, 1 (2015), 5:1–5:51.

[9] Kamalika Chaudhuri, Sanjoy Dasgupta, Samory Kpotufe, and Ulrike Von Luxburg. 2014. Consistent procedures for cluster tree estimation and pruning. *IEEE Transactions on Information Theory* 60, 12 (2014), 7900–7912.

[10] Gabor Csardi and Tamas Nepusz. 2006. The igraph software. *Complex syst* 1695 (2006), 1–9.

[11] H. A. David and J. Galambos. 1974. The Asymptotic Theory of Concomitants of Order Statistics. *Journal of Applied Probability* 11, 4 (1974), 762–770.

[12] Mark de Berg, Ade Gunawan, and Marcel Roeloffzen. 2019. Faster DBSCAN and HDBSCAN in Low-Dimensional Euclidean Spaces. *Int. J. Comput. Geom. Appl.* 29, 1 (2019), 21–47.

[13] Luc Devroye, László Györfi, and Gábor Lugosi. 2013. *A probabilistic theory of pattern recognition*. Vol. 31. Springer Science & Business Media.

[14] Matthijs Douze, Alexandr Guzhva, Chengqi Deng, Jeff Johnson, Gergely Szilvasy, Pierre-Emmanuel Mazaré, Maria Lomeli, Lucas Hosseini, and Hervé Jégou. 2024. The Faiss library. *arXiv* (2024). arXiv:2401.08281

[15] Mingjing Du, Shifei Ding, Yu Xue, and Zhongzhi Shi. 2019. A novel density peaks clustering with sensitivity of local density and density-adaptive metric. *Knowledge and Information Systems* 59 (2019), 285–309.

[16] Walid Durani, Dominik Mautz, Claudia Plant, and Christian Böhm. 2022. DBHD: Density-based clustering for highly varying density. In *2022 IEEE International Conference on Data Mining (ICDM)*. 921–926.

[17] Hossein Esfandiari, Vahab S. Mirrokni, and Peilin Zhong. 2021. Almost Linear Time Density Level Set Estimation via DBSCAN. In *AAAI*. 7349–7357.

[18] Martin Ester, Hans-Peter Kriegel, Jörg Sander, and Xiaowei Xu. 1996. A Density-Based Algorithm for Discovering Clusters in Large Spatial Databases with Noise. In *KDD*. 226–231.

[19] Junhao Gan and Yufei Tao. 2017. On the hardness and approximation of Euclidean DBSCAN. *ACM Transactions on Database Systems (TODS)* 42, 3 (2017), 1–45.

[20] Martijn Gösgens, Alexey Tikhonov, and Liudmila Prokhorenkova. 2021. Systematic Analysis of Cluster Similarity Indices: How to Validate Validation Measures. In *ICML*, Vol. 139. PMLR, 3799–3808.

[21] Sibylle Hess, Wouter Duivesteijn, Philipp Honysz, and Katharina Morik. 2019. The spectacl of nonconvex clustering: A spectral approach to density-based clustering. In *Proceedings of the AAAI conference on artificial intelligence*, Vol. 33. 3788–3795.

[22] Xiaogang Huang and Tiefeng Ma. 2023. Fast Density-Based Clustering: Geometric Approach. *SIGMOD* 1, 1 (2023), 58:1–58:24.

[23] Jennifer Jang and Heinrich Jiang. 2019. DBSCAN++: Towards fast and scalable density clustering. In *ICML*. 3019–3029.

[24] Heinrich Jiang. 2017. Density level set estimation on manifolds with dbscan. In *International Conference on Machine Learning*. PMLR, 1684–1693.

[25] Heinrich Jiang, Jennifer Jang, and Jakub Lacki. 2020. Faster DBSCAN via subsampled similarity queries. In *NeurIPS*.

[26] David R. Karger. 1999. Random Sampling in Cut, Flow, and Network Design Problems. *Math. Oper. Res.* 24, 2 (1999), 383–413.

[27] Stuart Lloyd. 1982. Least squares quantization in PCM. *IEEE transactions on information theory* 28, 2 (1982), 129–137.

[28] Son T. Mai, Ira Assent, and Martin Storgaard. 2016. AnyDBC: An Efficient Anytime Density-based Clustering Algorithm for Very Large Complex Datasets. In *KDD*. ACM, 1025–1034.

[29] Jirí Matousek. 1994. Geometric Range Searching. *ACM Comput. Surv.* 26, 4 (1994), 421–461.

[30] Mark EJ Newman. 2006. Modularity and community structure in networks. *Proceedings of the national academy of sciences* 103, 23 (2006), 8577–8582.

[31] Camilla Birch Okkels, Martin Aumüller, Viktor Bello Thomsen, and Arthur Zimek. 2025. High-dimensional density-based clustering using locality-sensitive hashing. In *EDBT*. 694–706.

[32] Ninh Pham. 2021. Simple Yet Efficient Algorithms for Maximum Inner Product Search via Extreme Order Statistics. In *KDD*. 1339–1347.

[33] Usha Nandini Raghavan, Réka Albert, and Soundar Kumara. 2007. Near linear time algorithm to detect community structures in large-scale networks. *Physical Review E—Statistical, Nonlinear, and Soft Matter Physics* 76, 3 (2007), 036106.

[34] Ali Rahimi and Benjamin Recht. 2007. Random Features for Large-Scale Kernel Machines. In *NIPS*. 1177–1184.

[35] Alex Rodriguez and Alessandro Laio. 2014. Clustering by fast search and find of density peaks. *science* 344, 6191 (2014), 1492–1496.

[36] Johannes Schneider and Michail Vlachos. 2017. Scalable density-based clustering with quality guarantees using random projections. *Data Min. Knowl. Discov.* 31, 4 (2017), 972–1005.

[37] Jianbo Shi and Jitendra Malik. 2000. Normalized Cuts and Image Segmentation. *IEEE Trans. Pattern Anal. Mach. Intell.* 22, 8 (2000), 888–905.

[38] Liping Sun, Fan Huang, Xiaoyao Zheng, Liangmin Guo, Qingying Yu, Zhenghua Chen, and Yonglong Luo. 2025. Density Peaks Clustering Based on Label Propagation and K-Mutual-Nearest Neighbors. *IEEE Transactions on Emerging Topics in Computational Intelligence* 9, 2 (2025), 1830–1842.

[39] Vincent A Traag, Ludo Waltman, and Nees Jan Van Eck. 2019. From Louvain to Leiden: guaranteeing well-connected communities. *Scientific reports* 9, 1 (2019), 1–12.

[40] Andrea Vedaldi and Andrew Zisserman. 2012. Efficient Additive Kernels via Explicit Feature Maps. *IEEE Trans. Pattern Anal. Mach. Intell.* 34, 3 (2012), 480–492.

[41] P. Viswanath and V. Suresh Babu. 2009. Rough-DBSCAN: A fast hybrid density based clustering method for large data sets. *Pattern Recognit. Lett.* 30, 16 (2009), 1477–1488.

[42] Shusen Wang, Alex Gittens, and Michael W. Mahoney. 2019. Scalable Kernel K-Means Clustering with Nyström Approximation: Relative-Error Bounds. *J. Mach. Learn. Res.* 20 (2019), 12:1–12:49.

[43] Roger Weber, Hans-Jörg Schek, and Stephen Blott. 1998. A Quantitative Analysis and Performance Study for Similarity-Search Methods in High-Dimensional Spaces. In *VLDB*. 194–205.

[44] HaoChuan Xu and Ninh Pham. 2024. Scalable DBSCAN with random projections. *NeurIPS* 37 (2024), 27978–28008.

[45] Bo Yang, Xiao Fu, Nicholas D Sidiropoulos, and Mingyi Hong. 2017. Towards k-means-friendly spaces: Simultaneous deep learning and clustering. In *international conference on machine learning*. PMLR, 3861–3870.

[46] Liu Yaohui, Ma Zhengming, and Yu Fang. 2017. Adaptive density peak clustering based on K-nearest neighbors with aggregating strategy. *Knowledge-Based Systems* 133 (2017), 208–220.

A Missing proofs

A.1 Proof of Theorem 2

From Theorem 1 [6], for $k \geq c \log n$, the mutual kNN graph is connected within each compact, connected component of a level set $\mathcal{L}_{f_i}$ with high probability.

Given a core point $\mathbf{x} \in C_i$, we have $d_k(\mathbf{x}) \leq \epsilon_i$. Let V_d be the volume of the unit ball in $\mathbb{R}^d$, by using the kNN density estimator [13]:

$$\widehat{f_k}(\mathbf{x}) = \frac{k}{nV_d \left(d_k(\mathbf{x})\right)^d},$$

we have $\widehat{f_k}(\mathbf{x}) \to f(\mathbf{x})$ uniformly under Lipschitz continuity. Since $\epsilon_i < (k/nV_d f_i)^{1/d}$, any core point $\mathbf{x}$ have $\widehat{f_k}(\mathbf{x}) > f_i$, and hence $\mathbf{x} \in \mathcal{L}_{f_i}$. Alternatively, for any point $\mathbf{x}$ with density $f_0 \leq f_i < f(\mathbf{x}) < f_{i+1}$, it will be identifying as a core point in the cluster C_i as $\epsilon_{i+1} < d_k(\mathbf{x}) < \epsilon_i$ and we run DBSCAN sequentially from ϵ_L to ϵ_1.

With consistent core point sets and identical connectivity structure within each cluster (via mutual kNN graph and ϵ_i-neighborhood graph), the connected components formed by $DBSCAN_k^*$ and mutual kNN graph are equivalent with high probability as $n \to \infty$. □

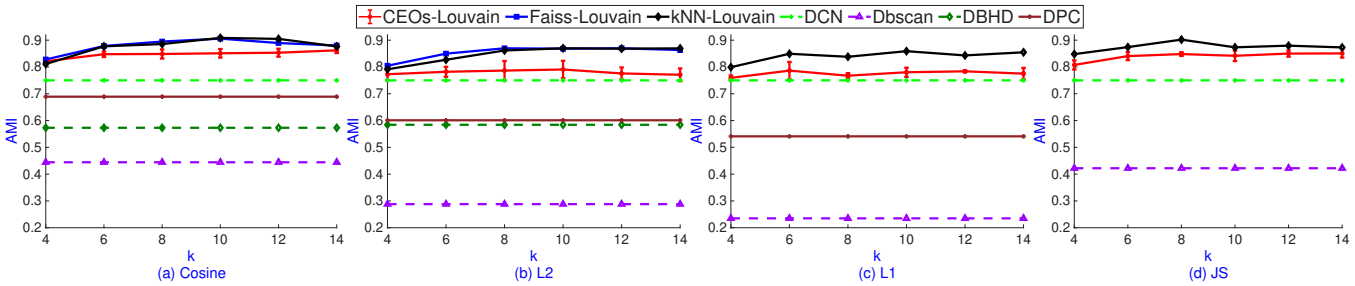

Figure 3: The AMI comparison of PING baselines (CEOs, FaissIVF, and exact kNN for graph constructions with Louvain) and other clustering competitors. We report the *best* AMI scores of compared competitors after tuning their parameters.

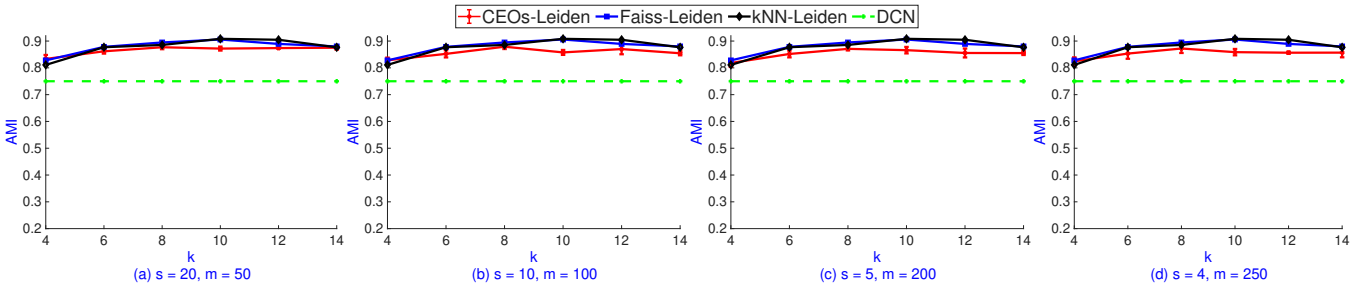

Figure 4: The AMI comparison of CEOs, FaissIVF, and exact kNN for graph constructions with Leiden and DCN. CEOs uses $D = 128$ and various values of s and m.

Table 7: The clustering accuracy comparison of CEOs-Leiden with $k = 8$ and several clustering competitors on cosine distance. We report the *best* scores of compared competitors after tuning their parameters.

Alg.	CEOs-Lei	sDbscan	Dbscan	Optics	HDBSCAN	DPC	DBHD	SpectACl	SC	KKM	k-means	DCN
NMI	**88% ± 1%**	42% ± 4%	43%	6%	31%	69%	54%	80%	50%	54%	51%	75%
ARI	**86% ± 2%**	9%	9%	0%	5%	54%	18%	70%	37%	41%	38%	62%
CC	**86% ± 1%**	15%	18%	0.3%	12%	57%	29%	71%	37%	41%	38%	64%

A.2 Proof of Lemma 3

Given a point $\mathbf{q} \in \mathbf{X}$, let $\mathbf{x}_k$ and $\mathbf{x}_m$ are top-k and top-m nearest neighbor of $\mathbf{q}$ in $\mathbf{X}$, respectively, where $m > k$.

Let $\alpha_q = \left(\mathbf{q}^\top \mathbf{x}_k - \mathbf{q}^\top \mathbf{x}_m\right) / \left(\sqrt{1-(\mathbf{q}^\top \mathbf{x}_k)^2} + \sqrt{1-(\mathbf{q}^\top \mathbf{x}_m)^2}\right)$, we will use the following lemma that show nearest neighborhood preservation asymptotically.

Lemma 6. *[32, 44] For two points $\mathbf{x}, \mathbf{q} \in \mathcal{S}^{d-1}$ and significantly large D random vectors $\mathbf{r}_i$, w.l.o.g. we let $\mathbf{r}_* = \arg\max_{\mathbf{r}_i} \mathbf{q}^\top \mathbf{r}_i$. Then, we have $\mathbf{x}^\top \mathbf{r}_* \xrightarrow{D} N\left(\mathbf{x}^\top \mathbf{q}\sqrt{2\ln(D)}, 1-(\mathbf{x}^\top \mathbf{q})^2\right)$.*

Let $X_k = \mathbf{x}_k^\top \mathbf{r}_*, X_m = \mathbf{x}_m^\top \mathbf{r}_*$ be random variable corresponding to the projection values of $\mathbf{x}_k, \mathbf{x}_m$ on $\mathbf{r}_*$, respectively. Then we have

$$X_k \sim N\left(\mathbf{q}^\top \mathbf{x}_k \sqrt{2\ln(D)}, 1-(\mathbf{q}^\top \mathbf{x}_k)^2\right),$$
$$X_m \sim N\left(\mathbf{q}^\top \mathbf{x}_m \sqrt{2\ln(D)}, 1-(\mathbf{q}^\top \mathbf{x}_m)^2\right).$$

Let $\alpha_q = \left(\mathbf{q}^\top \mathbf{x}_k - \mathbf{q}^\top \mathbf{x}_m\right) / \left(\sqrt{1-(\mathbf{q}^\top \mathbf{x}_k)^2} + \sqrt{1-(\mathbf{q}^\top \mathbf{x}_m)^2}\right)$, applying Chernoff bound on the Gaussian variable $X_m - X_k$ gives

$$\mathbf{Pr}\left[X_m \geq X_k\right] \leq D^{-\left(\mathbf{q}^\top \mathbf{x}_k - \mathbf{q}^\top \mathbf{x}_m\right)^2 / \left(\sqrt{1-(\mathbf{q}^\top \mathbf{x}_k)^2} + \sqrt{1-(\mathbf{q}^\top \mathbf{x}_m)^2}\right)^2} = D^{-\alpha_q^2}.$$

Let $\alpha_* = \arg\min_{\mathbf{q} \in \mathbf{X}} \alpha_q$. Since Lemma 6 holds for s closest random vectors $\mathbf{r}_i$ to $\mathbf{q}$ due to their asymptotic independence [11, 32], setting $D = n^{2/s\alpha_*^2}$, applying the union bound, we have the probability $\mathbf{x}_k$ is ranked higher than all points outside $mNN(\mathbf{q})$ over the s projections associated to the top-s vector closest to $\mathbf{q}$ is at least $1 - 1/n$.

Assuming that the event any point $\mathbf{x}_i \in kNN(\mathbf{q})$ is ranked higher than all $\mathbf{x}_j \in \mathbf{X} \setminus mNN(\mathbf{q})$ is independent, we have the probability that $kNN(\mathbf{q})$ are among top-m points associated to top-s closest random vector to $\mathbf{q}$ is at least $(1-1/n)^k \approx e^{-k/n}$. This proves the claim of Lemma 3.

Table 8: The total runtime in 32 threads and accuracy of CEOs, Faiss-IVF, and exact kNN in seconds with Louvain on cosine. CEOs uses $D = 256, s = 20, m = 50, k = 8$. Louvain takes 12 seconds.

Alg	Runtime (s)	Find kNN time (s)	AMI	CC
CEOs	15	3 (20% of time)	88% ± 1%	86% ± 1%
Faiss	35	23 (66% of time)	89%	86%
Exact	102	90 (88% of time)	90%	86%

B Extension to other similarity measures with random kernel features

We follow sDbscan approach [44] that extends CEOs to popular distance measures, including L2, L1, χ^2, and Jensen-Shannon (JS). We will utilize the random kernel feature mappings f [34, 40] to embed these distances into cosine distance, i.e. $f : \mathbb{R}^d \mapsto \mathbb{R}^{d'}$ such that $\mathbf{E}\left[f(\mathbf{x})^\top f(\mathbf{q})\right] = K(\mathbf{x}, \mathbf{q})$ where K is the kernel function. We use Gaussian, Laplacian, χ^2, and JS kernels as their randomized mappings are well-studied and efficiently computed. Similar to sDbscan, the embeddings cost is negligible compared to the distance computation in CEOs.

We present the well-known random Fourier embeddings [34] for K_G with $\sigma = 1$. We first generate d' random vectors $\mathbf{w}_i, i \in [d']$ whose coordinates are from $N(0, 1)$. Our randomized mappings are:

$$f(\mathbf{x}) = \frac{1}{\sqrt{d'}}\{\sin(\mathbf{w}_i^\top \mathbf{x}), \cos(\mathbf{w}_i^\top \mathbf{x}) \mid i \in [d']\} \in \mathcal{S}^{2d'-1}.$$

By Hoeffding's inequality, we can show that $d' = O(\log(n))$, the randomized mapping f preserves well the kernel function of every pair of points, and hence preserve the quality of clustering structure.

C Parameter settings

We detail the parameter setting of studied clustering method.

DPC [2]: We determine the number of clusters based on threshold values $\rho_{min}, \delta_{min} \in [0.05, 0.5]$, where both ρ and δ are normalized. The cutoff distance d_c is chosen such that the average $|\overline{B}_{d_c}(\mathbf{x}_i)| \in [0.01, 0.02] \cdot n$. Note that DPC requires all pairwise distances that need 30GB memory to store to run efficiently.

DCN [3]: We set the latent dimensionality to 10, both the number of epochs and pre-training epochs are set to 50. The regularization coefficient λ is 0.005, and the learning rate is fixed at 0.002.

DBHD [4]: We set $\rho, \beta \in [0.3, 0.7]$ and $minClusterSize \in [4, 32]$. We replace the original kd-tree based exact KNN implementation with exact Faiss and observe that it speeds up the running time by 1.3×.

SpectACl [5]: We choose the target cluster number ($n\_clusters$) is 10, and set ε as the smallest radius such that 90% of the points have at least 10 neighbors, with additional nearby values also considered. Besides, the embedding dimensionality is set to default value 50. This version suffers small AMI score of 45%.

[2]https://github.com/pgoltstein/densitypeakclustering
[3]https://github.com/guenthereder/Deep-Clustering-Network
[4]https://dm.cs.univie.ac.at/research/downloads
[5]https://sfb876.tu-dortmund.de/spectacl

Table 9: Runtime of CEOs-DNP components in seconds with $D = 128, s = 10, m = 50, k = 8$, on Mnist with multi-threads.

Threads	Indexing	Finding neighbors	DNP	Total
1	1.21	16.04	0.53	17.83
8	0.27	2.75	0.54	3.60
16	0.19	1.76	0.55	2.55
32	0.15	1.3	0.53	2.05

Table 10: Breakdown runtime of Faiss-IVFPQ and CEOs with different propagation algorithms on Pamap2.

Alg.	IVF-Lei	IVF-DNP	IVFPQ-Lei	CEOs-DNP
Find kNN (s)	121	121	42	24
Build graph (s)	74	0	84	0
Propagation (s)	121	3	98	37
Total time (s)	316	124	346	**61**

SpectACl (Normalized) [5]: This variant replaces $\varepsilon-neighborhood$ graph with KNN graph to construct the normalized adjacency matrix. We vary the value of K in [5, 10, 15, 20]. The target cluster number ($n\_clusters$) is also 10, and the embedding dimensionality remains at the default value of 50. This version gives 80% AMI score is used in comparison with PING.

DBSCAN [6]: We choose $\epsilon \in [0.08, 0.12]$ (for cosine distance), and $\epsilon \in [1000, 1300]$ (for L2 distance), $minPts \in [4, 32]$.

OPTICS [7]: We choose ϵ is 0.8 for cosine distance, 2400 for L2 distance , $minPts \in [12, 32]$, $Xi \in [0.001, 0.005]$.

Kernel k-means (KKM) and spectral clustering (SC): Due to the limit of memory, we use the Nyström approach with 1000 samples for acceleration and for estimating the scale σ used in the kernel.

HDBSCAN [8]: We use the default value $minClusterSize = 30$. HDBSCAN does not support multi-threading.

D Additional experimental results on Mnist

Louvain. Figure 3 shows the comparison in clustering accuracy between PING baselines with Louvain and other clustering methods. Again, we report the best AMI score after tuning their parameters. The results given by Louvain is very similar to that of Leiden over 4 studies distance measures.

Table 8 shows the breakdown cost of graph constructions with CEOs, Faiss-IVF and exact KNN with Louvain. It is clear that constructing graph with Faiss is a computational bottleneck as it constitute to 66% of total cost.

Sensitivities of s, m of CEOs. Figure 4 shows a similar output of PING baselines with different graph construction and Leiden. We set various parameter s, m of CEOs to verify the sensitivity. Over a

[6]https://scikit-learn.org/stable/modules/generated/sklearn.cluster.DBSCAN.html
[7]https://scikit-learn.org/stable/modules/generated/sklearn.cluster.cluster_optics_xi.html
[8]https://hdbscan.readthedocs.io/en/latest/

Table 11: AMI and runtime comparison between CEOs-DNP and Dbscan variants with L1 on Pamap2.

Alg.	CEOs-DNP	Dbscan	sDbscan	sngDbscan
AMI	51%	48%	48%	40%
Runtime (min)	1.2	30	1	3

Table 12: Sensitivity of c, k' on Faiss-IVF-DNP on Pamap2 with L2.

Param.	$c = 1$ $k' = 36$	$c = 2$ $k' = 18$	$c = 3$ $k' = 12$	$c = 4$ $k' = 4$	$c = 5$ $k' = 4$	$c = 5$ $k' = 5$
AMI	47%	48%	50%	51%	51%	52%

wide range of s, m, CEOs-Leiden still outperforms DCN with up to 10%.

Other clustering metrics. Table 7 shows that CEOs-Leiden provides a superior clustering accuracy measured by NMI, ARI, and CC compared to many clustering baselines.

Multi-threading CEOs-DNP. Table 9 shows the breakdown cost of different components of CEOs, including building index, finding neighbors, and label propagation with DNP. Similar to Louvain and Leiden, DNP does not run in multi-threading. However, the main computational cost is still on distance computation step in finding approximate kNN. Fortunately, it can be sped up with multi-threading, achieving up to 12× with 32 threads.

E Additional experimental results on Pamap2

Runtime of different components of PING. Table 10 shows the breakdown cost for different components, including finding kNN, building neighborhood graph, and propagation of ANNS and different propagation algorithms. It is clear that CEOs runs significantly faster than Faiss-IVF and Faiss-IVFPQ while DNP is faster than Leiden. On small graph $k = 12$, DNP runs in 3 seconds while Leident need 2 minutes. Even on larger graphs, e.g. $k = 75$ for CEOs-DNP, and $k = 250$ for Faiss-IVFPQ, Leiden is still slower than DNP.

Comparison on L1 between CEOs-DNP and DBSCAN variants. Table 11 shows the comparison between CEOs-DNP and other DBSCAN variants. CEOs uses $D = 512, s = 20, m = 50$ while DNP uses $k = 100$ with $c = 5$ and $k' = 20$. CEOs-DNP achieves higher accuracy than Dbscan variants though sharing similar running time with sDbscan.

Sensitivity of c, k' of DNP. We run Faiss-IVFPQ to create the graph G_k where $k = ck'$ with different value of $c = \{1, 2, 3, 4, 5\}$ and $k' = \{36, 18, 12, 4\}$. Table 12 shows the sensitivity of c, k' of DNP. It demonstrates the function of c on effectively controlling the trade-off between neighborhood connectivity and local density estimation: smaller values of c emphasize finer local density variations, while larger values allow broader neighborhood influence during propagation. Table 13 shows the stable accuracy of CEOs-DNP while fixing $c = 5$ and varying $k = ck'$.

Table 13: Sensitivity of k' on CEOs-DNP on Pamap2 when fixing $c = 5$ with L2.

k'	10	15	20	25	50	75	100
AMI	46%	47%	47%	48%	48%	48%	48%

Table 14: Sensitivity of c, k' on Faiss-IVFPQ-DNP on Mnist8m with cosine.

Param.	$c = 2$ $k' = 100$	$c = 4$ $k' = 25$	$c = 4$ $k' = 30$	$c = 4$ $k' = 35$	$c = 5$ $k' = 20$	$c = 5$ $k' = 25$
NMI	60%	62%	70%	72%	67%	66%

F Additional experimental results on Mnist8m

Sensitivity of c, k' of DNP. We run Faiss-IVFPQ with $k_{max} = 200$ and create the graph G_k where $k = ck'$ with different value of $c = \{2, 4, 5\}$ and $k' = \{20, 25, 30, 35\}$. Table 14 shows the sensitivity of c, k' of Faiss-IVFPQ-DNP. Though the NMI score is different at most 10%, these values are significantly higher than kernel k-means with NMI of 41% though the runtime is still under 15 minutes.

Time-accuracy trade-offs. Table 15 show the time-accuracy trade-off of Faiss-IVFPQ with Leiden when varying k. The higher k leads to higher clustering accuracy but higher runtime due to the increasing cost of graph construction and modularity score evaluation.

Table 15: Time and accuracy of Faiss-IVFPQ Leiden with various of k on Mnist8m using cosine.

k	10	12	14	16	18	20	DNP
AMI	54%	59%	64%	69%	72%	73%	72%
Time (min)	37	40	44	49	54	57	**15**